water

MDPI

Article

Design and Preparation of Magnetically-Oriented Poly(styr-co-MMA)-3MPS Capped Fe(ZnO) Hybrid Microspheres for Ion Exchange Removal of Toxic Pollutants from Wastewater

Sahar Fatima [1], Muhammad Imran [1,*], Farah Kanwal [2], Ayesha Javaid [1], Shoomaila Latif [3] and Grzegorz Boczkaj [4,5,*]

[1] Centre for Inorganic Chemistry, School of Chemistry, University of the Punjab, Lahore 54000, Pakistan
[2] Centre for Physical Chemistry, School of Chemistry, University of the Punjab, Lahore 54000, Pakistan
[3] School of Physical Sciences, University of the Punjab, Lahore 54000, Pakistan
[4] Department of Sanitary Engineering, Faculty of Civil and Environmental Engineering, Gdańsk University of Technology, G. Narutowicza 11/12 Str., 80-233 Gdańsk, Poland
[5] EkoTech Center, Gdańsk University of Technology, G. Narutowicza St. 11/12, 80-233 Gdańsk, Poland
* Correspondence: imran.hons@pu.edu.pk (M.I.); grzegorz.boczkaj@pg.edu.pl (G.B.)

Abstract: In this work, polymeric microspheres derived from polystyrene-co-methyl methacrylate embedded with magnetic ZnO nanoparticles (poly(styrene-co-MMA)-3MPS-Fe (ZnO)) were synthesized using the suspension polymerization method. The surfaces of polymeric Fe(ZnO) microspheres were improved by functionalization with amino and sulphonate groups. The physicochemical analysis indicated a large number of positively charged (anion exchange) groups (91 mmol/g) on the amine-modified polymeric microsphere (MFZPI) and a large number of negatively charged (cation exchange) groups (90 mmol/g) on the sulphonate-modified polymeric microsphere (SMFZPI)—revealing ambivalent character of obtained sorbent. The characterization of the synthesized compounds using various analytical techniques such as TGA, FTIR, XRD, SEM/EDX, UV-VIS and VSM indicated that synthesized microspheres were thermally stable, semi-crystalline in structure with hollow irregular morphology, optically active in UV region and slightly magnetic in nature. Due to the introduction of groups having ion exchange properties, these modified poly(styrene-co-MMA)-3MPS-Fe(ZnO) microspheres were used for the ion exchange sorptive removal of Cr(III) and fluorescein from aqueous matrix. The equilibrium sorption capacity of Cr(III) was 16.79 mg/g whereas of fluorescein was 12.03 mg/g under optimized conditions. Therefore, SMFZPI was found to be a promising sorbent for both cationic heavy metals and anionic dyes due to the presence of both acidic and basic groups. The mathematical modelling revealed that the sorption phenomenon followed pseudo-second-order kinetics with Freundlich equilibrium isotherm, indicating multilayer chemisorption of the pollutants on the synthesized ion exchange sorbents. This work establishes the utilization of polymeric magnetic ZnO-based ion exchange sorbents to effectively remove harmful toxins from wastewater.

Keywords: polymerization; water treatment; adsorption; polymeric materials; surface functionalization; contaminants of emerging concern

check for updates

Citation: Fatima, S.; Imran, M.; Kanwal, F.; Javaid, A.; Latif, S.; Boczkaj, G. Design and Preparation of Magnetically-Oriented Poly(styr-co-MMA)-3MPS Capped Fe(ZnO) Hybrid Microspheres for Ion Exchange Removal of Toxic Pollutants from Wastewater. *Water* **2023**, *15*, 1761. https://doi.org/10.3390/w15091761

Academic Editors: Abdollah Dargahi and Amir Shabanloo

Received: 27 March 2023
Revised: 25 April 2023
Accepted: 30 April 2023
Published: 3 May 2023

1. Introduction

During past decades, the increased urbanization has resulted in the haphazard dumping of hazardous materials in water/soil ecosystems. This practice has deteriorated our environment, consequently affecting the whole living community through food chains. Heavy metals and organic dyes from tanneries, electric power plants and textile industries are water soluble and cause deleterious effects even at low concentrations [1,2]. Cr(III) is the 17th most abundant metal on earth, beneficial for human health, but its high concentrations may create adverse health problems due to its oxidative conversion to more potent Cr(VI).

Similarly, textile and dyeing industrial effluents are also accountable for adding 100 tons of dyes/year to water ecosystems. For instance, fluorescein, an anionic hydrophilic dye with polyaromatic rings, has also proven hazardous at high concentrations. Its complexes are non-biodegradable and stable towards environmental fluctuations, making them more vulnerable pollutants and should be eliminated before entering water bodies [3]. This scenario demands a dire need to design some cost-effective, environment-friendly and easy-to-approach strategy to cope with this burning issue of water pollution.

Target pollutants are degraded via advanced oxidation processes (AOPs) [4–6]. On the other hand, techniques such as adsorption, ion exchange, coagulation, precipitation, filtration and solvent extraction have been used previously for batch/column removal of toxic contaminants. Among these, ion exchange adsorption has received much attention as a handy technique owing to its high sustainability and versatile, economic adsorbent application [7,8]. Ion exchange adsorption is the ion exchange process of concentrating and deposing target pollutants on the surface of the substrate with respect to the surface charge distribution, i.e., the removal of anion pollutants via anion exchange adsorbents and vice versa. In terms of adsorbent selection, polymeric organic-inorganic hybrid microspheres (0.1–100 μm) have received considerable attention due to the relatively easy adjustment of grain size and surface area by regulating reaction conditions [9]. The inorganic nanoparticles inside the polymeric framework have higher efficiency, increased durability and improved selectivity than sole nanoparticles. For example, ZnO nanoparticles have been reported for their enlarged surface area, good biocompatibility and remarkable adsorptive activity [10]. Moreover, doping ZnO by magnetic materials such as cobalt, nickel, and iron can further increase its mechanical functioning by improving its optical and magnetic properties. Introducing such magnetic nanoparticles in polymers provides an emerging approach towards environmental remediation. The polymeric shell surrounding the magnetic metal core prevents the secondary pollution caused by metal (magnetic) leakage in the solution [11]. For the good dispersion of metal with in polymer network to restrict the outflow of magnetic particles, certain organic groups may also be grafted on metal surfaces such as oleic acid or silane coupling agent etc. Depending on the type of functional group, these magnetic polymer microspheres can be applied as ion exchange adsorbents (cation/anion) to facilitate water purification. The recently published literature investigated the effective adsorption of tartrazine azo dye by magnetic Fe_2O_3-based polystyrene–divinyl benzene composite [12]. Sulphonate (–SO_3H) modified magnetic chitosan–polystyrene are also reported for decontaminating methylene blue dye via adsorption [13].

Considering the above-narrated literature, the present work focuses on synthesising Fe-doped ZnO magnetic nanoparticles copolymerized with styrene and methyl methacrylate. Further, the polymer-embedded Fe(ZnO) microspheres were functionalized with amino and sulphonic groups to induce ion exchange ability. The ion exchange adsorption of the said materials has been investigated against the removal of Cr(III) and fluorescein. The optimization of various parameters influencing the adsorption capacity has also been done, along with applying mathematical models to get insights into the ion exchange adsorption of Cr(III) and fluorescein.

2. Materials and Methods

Details about the chemical reagents used in the present work are provided in Text S1.1 of the Supplementary Materials.

2.1. Synthesis of Ion Exchange Functionalized Magnetic Poly(styr-co-MMA)-3MPS Capped Fe(ZnO) Hybrid Microspheres

The polymeric microspheres of magnetic ZnO were synthesized in three distinct steps. Initially, Fe-doped ZnO were prepared by reported sol-gel method with some modifications (Scheme S1, Step 1) [14] followed by the silane-coating of Fe(ZnO) in the second step using the reported procedure of Bach et al. [15]. The third step involved the copolymerization of 3MPS-Fe(ZnO) nanoparticles with styrene and methyl methacrylate using oil-water suspension polymerization (Scheme S1, Step 3) [16]. Further, the functionalization of co-polymerized silane-modified magnetic ZnO was carried out according to the reported methods [17]. The detailed synthesis procedure is provided in Text S1.2 & S1.3 of the Supplementary Materials.

2.2. Characterization

The synthesized materials were characterized using various analytical techniques. Text S1.5 of Supplementary Materials provides the complete information.

2.3. Batch Ion Exchange Adsorption of Cr(III) and Fluorescein

The ion exchange adsorption of Cr(III) and fluorescein (10 ppm, 10 mL) with MFZPI/SMFZPI (30 mg) were investigated individually in a single metal/dye system by optimizing the parameters influencing the adsorption capacity. The effect of pH was estimated within the pH range of 2–12 using HCl (0.1 M) and NaOH (0.1 M). The rate of Cr(III) and fluorescein sorption was also investigated at different contact times of 20, 40, 60, 80, 120 and 180 min at optimum pH to study the influence of contact time of adsorbent on the adsorptive removal of the said pollutants. The effect of initial metal/dye concentration on the sorption rate of Cr(III) and fluorescein was studied at initial concentrations in the range of 20–80 ppm by keeping other parameters constant. The influence of temperature changes on the batch ion exchange sorption of Cr(III) and fluorescein with anionic MFZPI and cationic SMFZPI adsorbents were studied in the temperature range of 293–333 K. All the experiments were done in replicates at an agitation speed of 250 rpm, the solutions were filtered, and the filtrates were investigated by atomic absorption spectroscopy (AAS) for Cr(III) sorption and visible spectrophotometer for fluorescein removal. The maximum sorption (q_e, mg/g) and removal percentage (R%) of Cr(III) and fluorescein by MFZPI and SMFZPI were estimated with the following equations [18] (Equations (1) and (2)).

$$q_e = \frac{(C_o - C_e)}{m} \cdot V \tag{1}$$

$$R\% = \left(\frac{C_o - C_e}{C_o}\right) \cdot 100 \tag{2}$$

where, C_o = initial concentration, C_e = Equilibrium concentration, V = volume of solution, and m = mass of ion exchange sorbent.

2.4. Kinetic Modeling

The kinetics of the synthesized ion exchange adsorbents was studied against Cr(III) and fluorescein using Elovich, pseudo-first-order, pseudo-second-order and intraparticle diffusion kinetic models. The following linear equations were used to determine the sorption rates with respect to the time (Equations (3)–(6)) [18].

$$q_t = \frac{1}{b} \ln ab + \frac{1}{b} \ln t \tag{3}$$

$$\ln\left(q_e - q_t\right) = \ln q_e - K_1 t \tag{4}$$

$$\frac{t}{q_t} = \frac{1}{K_2 . q_e^2} + \frac{t}{q_e} \tag{5}$$

$$q_t = K_{in}\, t^{1/2} + C \tag{6}$$

where, q_t (mg/g) and q_e (mg/g) represent sorption of Cr(III)/fluorescein at a time "t" and at equilibrium, respectively. The K_1, K_2 and K_{in} are the pseudo-first-order, pseudo-second-order and intraparticle diffusion rate constants. The constant "a" denotes the initial absorption rate, and "b" indicates the surface coverage and activation energy related to the chemisorption.

2.5. Equilibrium Modeling

The quantitative representation of solute–sorbent equilibrium at constant temperature was investigated using three isotherms i.e., Langmuir isotherm (Equation (7)), Freundlich isotherm (Equation (8)) and Dubrinin-Radulskawich (D–R) isotherm (Equation (9)). The linear equations are as follows.

$$\frac{C_e}{q_e} = \frac{C_e}{q_{max}} + \frac{1}{K_L . q_{max}} \quad (7)$$

$$\ln\ q_e = \ln\ K_f + \frac{1}{n} \ln C_e \quad (8)$$

$$\ln\ q_e = \ln\ q_{max} - \ \beta \varepsilon^2 \quad (9)$$

$$E = \frac{1}{\sqrt{2\beta}} \quad (10)$$

where q_e is the equilibrium sorption of Cr(III) and fluorescein dye, C_e (mg/L) represents the equilibrium concentration of Cr(III) and fluorescein dye, K_L/K_f are the Langmuir/Freundlich equilibrium constant representing the sorbate affinity for binding sites, 1/n denotes adsorption energy distribution referring to better (n = 2–10), good (n = 1–2) and average (<1) adsorption and β is the polynai constant [19]. The mean free energy "E" (kJ/mol) given in Equation (10) was used to investigate the type of sorption mechanism i.e., E < 8 represents weak physiosorption and E > 8 shows chemisorption between sorbate and sorbent.

2.6. Thermodynamic Modeling

The thermodynamics of Cr(III) and fluorescein sorption on MFZPI and SMFZPI was investigated with Gibb's free energy (ΔG°) equation (Equation (11)).

$$\Delta G^\circ = \Delta H^\circ - T\Delta S^\circ \quad (11)$$

where, ΔG° = Gibb's free energy, its negative value represents reaction spontaneity, and positive ΔG° represents non–spontaneous sorption, ΔH° = enthalpy that signifies the exothermic (negative ΔH°) and endothermic (positive ΔH°) nature of the sorption, ΔS° = entropy which explains the randomness at the sorption interface. Moreover, negative ΔS° represents decreased entropy, and positive ΔS° gives the structure changes in the sorbent with increased entropy [18].

2.7. Statistical Analysis

The results obtained in three replicates were given as mean values ± standard deviations using statistical progress, version 5.1. The deviations were examined by one-way analysis of variance (ANOVA). The coefficient of determination ($R^2 - 1$) was determined, and its adequacy was estimated by comparing F calculated with F obtained, i.e., lack of fit test.

3. Results and Discussions

The Fe-doped ZnO magnetic nanoparticles were synthesized by the sol-gel method and further copolymerized with styrene and methyl methacrylate, followed by the functionalization with amino and sulphonic groups. The synthesized amino functionalized microspheres (MFZPI) and sulphonic functionalized microspheres (SMFZPI) were in powdered form and obtained in good yields. The physicochemical analysis of these ion-exchange sorbents, i.e., MFZPI and SMFZPI, predicted the concentration of total acidic/basic groups on the sorbent surface. According to Boehm's titrations, the total acidic and basic groups present on the surface of MFZPI were 53.14 mmol/g and 91 mmol/g, respectively, reflecting the high concentration of basic groups on polymeric microsphere due to the attachment of the amine group. On the other hand, the amount of total acid and base groups on SMFZPI was 90 mmol/g and 83.2 mmol/g, respectively, depicting a large amount of acidic groups that may impart a negative surface charge to it. Thus, MFZPI contains a positive surface charge and can act as an anion exchange adsorbent for the negatively charged pollutants, whereas SMFZPI can act as a cation exchange adsorbent to attract the positively charged toxins. Further characterization and adsorption studies confirmed this hypothesis, and results are as follows.

3.1. FTIR Analysis

The FTIR spectrum of Fe-doped ZnO showed broad absorptions band at 3743 cm^{-1}, 1293 cm^{-1} and 1600 cm^{-1} representing the –OH bending vibrations due to the adsorbed water [20]. The small peaks observed around 835 cm^{-1} and 675 cm^{-1} were attributed to the vibrational frequencies caused by the incorporation of iron in the ZnO lattice [21]. The surface coating of magnetic ZnO with silane was confirmed by the appearance of strong peaks of Si-O at 1107 cm^{-1}, 936 cm^{-1} and 1018 cm$^{-1,}$ whereas C-O-C vibrations at 1306 cm$^{-1,}$ along with the absorption peaks of Fe(ZnO) also indicated the surface modification of ZnO. A sharp vibrational peak at 1700 cm^{-1} and a weak vibrational peak at 1623 cm^{-1} represented the C=O and C=C conjugating groups of the silane coupler [15]. Further, copolymerization of the 3MPS coated Fe(ZnO) with styrene and MMA was confirmed by the appearance of a strong intensity peak of C=O of the ester group appeared at 1727 cm^{-1} and some medium intensity absorption peaks in the range of 1520–1400 cm^{-1} attributed to the aromatic C=C vibrations of styrene [22]. Some other new peaks of C–H stretching at 3000–2866 cm^{-1} and out-of-plane bending at 758 cm^{-1} and 693 cm^{-1} indicated the attachment of MMA [23]. These results are in agreement with the FTIR study of Frizzo et al. regarding zinc oxide nanoparticles, copolymerized with MMA and styrene using miniemulsion polymerization technique [24]. Ethylenediamine functionalization of poly(styr-co-MMA)-3MPS-Fe(ZnO) (MFZPI) was confirmed by strong vibrational frequency of –NH_2 at 3600–3100 cm^{-1} and –NH bending vibrations at 1659–1550 cm^{-1} [25]. In case of SMFZP1, the peaks around 3400 cm^{-1} represented the presence of –SO_3H group in addition to the vibrational frequencies of MFZPI indicating the successful sulphonation of MFZPI (Figure S1). The vibrational bands around 1181 cm^{-1} and 1003 cm^{-1} were attributed to the S=O symmetrical stretching vibrations. Moreover, the substitution of benzene ring with the sulphonic group was also confirmed by the peaks that appeared at 892 cm^{-1}, 840 cm^{-1} and 663 cm^{-1} corresponding to the S–O group [26]. The obtained FTIR spectrum of SMFZP1 was supported by the earlier study of Kugarajah et al. for the sulphonated co-polymerized ZnO nanorods [27].

3.2. UV-Vis Spectroscopy

The UV-Vis spectra of synthesized materials were recorded in the range of 200–400 nm at room temperature (Figure S2). The Fe(ZnO) nanoparticles showed an absorption maximum at 245 nm owing to the electronic excitations from n–π or σ–π orbitals [28]. The coupling of silane group (3MPS) with Fe(ZnO) showed another small shoulder peak at 238 nm which is because of the absorbance of Si–O groups. The co-polymerization of 3MPS–Fe(ZnO) with styrene and methyl methacrylate resulted in the peak broadness due to electron jump between n–π and n–π* orbitals. This broad spectral response is also attributed to the variation in the local environment of the 3MPS–Fe(ZnO) induced by the substitution of some of the metal oxygen linkages with the polymeric framework [29]. Functionalization of poly(styr-co-MMA)-3-MPS-Fe(ZnO) with ethylenediamine (MFZPI) displayed the similar UV-Vis absorption spectrum with slight shifting of λ_{max} (250 nm) and more peak broadening was observed indicating the structural modifications in the polymerized magnetic ZnO which are responsible for this behavior. The UV-Vis spectrum of SMFZPI displayed broadest peak among all samples and it also shifted towards shorter wavelength, suggesting that –SO_3H functionalization to magnetic hybrid microspheres enhances their UV shielding properties [30].

3.3. SEM–EDX Analysis

The morphological features of the fabricated samples were studied by obtaining SEM micrographs (Figure 1). The Fe-doped ZnO nanoparticles obtained by the sol gel method showed non-uniform spherical shaped morphology (Figure 1a) in accordance with the previous report [31]. The capping of Fe(ZnO) with silane was reflected by the agglomeration of the spherical particles along with some visible small grains on the surface indicating the surface modification of Fe(ZnO) due to the attachment of silane (Figure 1b). The SEM micrograph of the copolymerized-surface modified magnetic zinc oxide is shown in Figure 1c. It depicted agglomerated sheet like morphology revealing the transition of zinc oxide structure from crystalline to amorphous form owing to the amorphous nature of incorporated polymers. The functionalization of poly(styr-co-MMA)-3MPS-Fe(ZnO) with ethylenediamine followed by the sulphonation constituted the non-uniform hollow surface arrangements with increased outward active sites (Figure 1d,e). These findings were in agreement with the finger like hollow morphology of the reported ZnO/Polyvinylidene difluoride (PVDF) membranes [32]. Such type of irregular/hollow surfaces having enormous active sites may induce excellent ion exchange adsorptive potential to the synthesized material to trap waste compounds [33].

The EDX analysis showed the elemental composition of the synthesized microspheres. The Fe-doped ZnO showed the presence of Zn, O and Fe with atomic percentages of 49.98 at.% 38.13 at.%, and 11.99 at.%, respectively (Figure S3a). The EDX profile of 3-MPS-Fe(ZnO) revealed the precision of the synthesis due to the appearance of new silicon and carbon peaks owing to $H_3C–C=CH_2$ bonded silane (Si–O) in 3MPS compound having C (54.51 at.%), O (32.05 at.%), Si (11.4 at.%), Zn (1.49 at.%), and Fe (0.3 at.%) (Figure S3b). The inclusion of polymers in the copolymerized-3MPS-Fe (ZnO) was verified by appearance of only desired elemental peaks of C (36.54 at.%), O (73.14 at.%), Zn (34.93 at.%), Si (1.9 at.%), and Fe (0.5 at.%) (Figure S3c). Figure S3d,e shows the emergence of new elemental peaks of N (3.2 at.%) and S (1.79 at.%) that confirmed the successful amination and sulphonation of the MFZPI and SMFZPI, respectively.

3.4. XRD Analysis

The X-ray diffraction pattern specifically demonstrates the crystallinity and particle size of the materials. Figure 2 compares the XRD patterns of the synthesized compounds. The appearance of XRD peaks of Fe(ZnO) at 31.8°, 34.3°, 36.25°, 47.45°, 56.45°, 62.75°, 66.15°, 67.82° and 69.19° were indexed at (100), (002), (101), (102), (110), (103), (200), (112), respectively, in accordance with JCPDS card no = 36–1451 as reported in the literature [20]. The smaller intensity of appeared peaks and peak shifting as compared to pristine ZnO indicated the successful doping of Fe in the ZnO crystals. The particle sizes were calculated as per Debye—Scherrer formula using Equation (12).

$$D = K\lambda/\beta\cos\theta \tag{12}$$

where, k, λ, β and θ are Scherrer's constant, X-rays wavelength, full width at half maxima and Bragg's angle, respectively [32]. The average particle size of Fe(ZnO) was found to be 44 nm indicating the formation of nanosized Fe(ZnO). The XRD pattern for 3MPS-Fe(ZnO) showed similar peaks as observed for Fe(ZnO) with decreased intensity. It is evident that addition of 3MPS did not alter the crystal structure of Fe(ZnO), however, the crystallite size was reduced to 41 nm in agreement with the reported literature [34]. Addition of poly(styr-co-MMA) into the 3MPS-Fe(ZnO) was confirmed by appearance of only two peak at 31.80° and 45.40° indicating the reduced crystallinity. Furthermore, the crystallite size was dramatically minimized to 3.05 nm. This decrease in particle size was due to polymer reaction conditions which improved the uniformity and narrowed the particle size. The XRD spectrum of EDA modified poly(styr-co-MMA)-3MPS-Fe (ZnO) depicted a high intensity peak at 19.89° corresponding to the lattice plane of (001). The peak design indicated semi–crystalline material formation after EDA addition and the results are found compatible with previously reported literature [35]. Few other small intensity diffraction peak at 45.46° and 66.07° were due to Fe(ZnO). Sulphonated-EDA modified poly(styr-co-MMA)-3MPS-Fe (ZnO) showed crystalline peaks of small intensities at 30.33°, 35.64°, 43.11°, 57.2° and 69.6° indicating decreased amorphous character as compared to poly(styr-co-MMA)-3MPS-Fe(ZnO) and particle size in nanometer range i.e., 5.2 nm. These findings are in agreement with the SEM micrographs which also revealed the similar results i.e., SMFZPI showed agglomerated hollow spheres with increased surface active sites and decreased amorphous character.

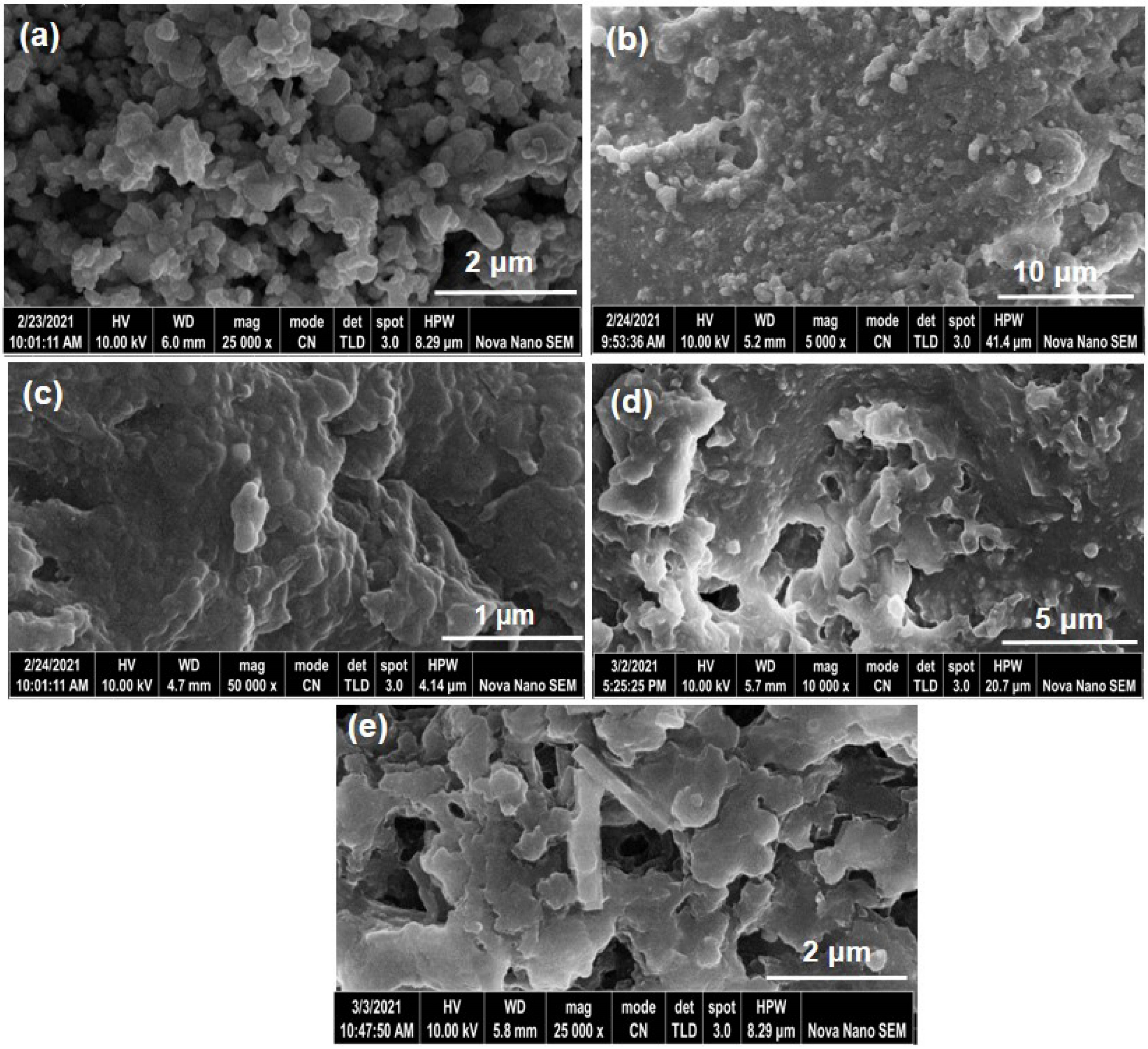

Figure 1. SEM micrographs of (**a**) Fe(ZnO), (**b**) 3-MPS-Fe(ZnO), (**c**) poly(styr-co-MMA)-3MPS-Fe(ZnO), (**d**) EDA-poly(styr-co-MMA)-3MPS-Fe(ZnO) (MFZPI), and (**e**) Sulphonated-EDA-poly(styr-co-MMA)-3MPS-Fe(ZnO) (SMFZPI).

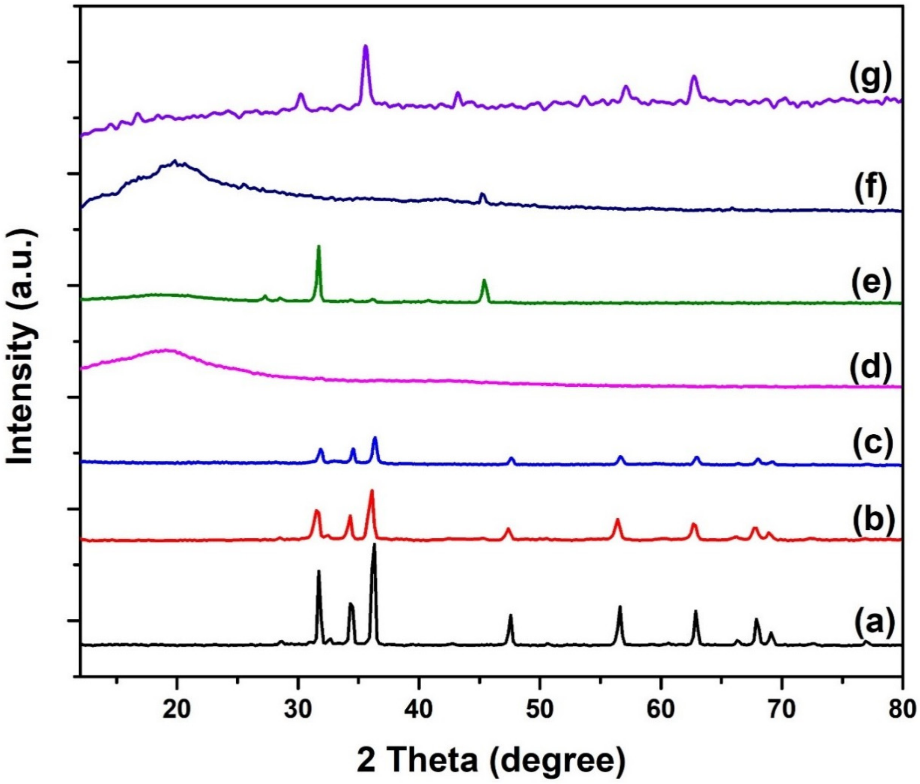

Figure 2. XRD pattern of (a) ZnO, (b) Fe(ZnO), (c) 3-MPS-Fe(ZnO), (d) poly(styr-co-MMA) (e) poly(styr-co-MMA)-3MPS-Fe(ZnO), (f) EDA-poly(styr-co-MMA)-3MPS-Fe(ZnO) (MFZPI), and (g) Sulphonated-EDA-poly(styr-co-MMA)-3MPS-Fe(ZnO) (SMFZPI).

3.5. Thermogravimetric Analysis

The thermal stability of the synthesized samples were investigated from their thermogravimetric curves recorded in the range 20–500 °C (Figure S4). Fe(ZnO) showed a small weight loss of 0.78% upto 120 °C due to the loss of adsorbed water molecules. The second weight loss of 71% was observed in the temperature range of 250–385 °C and attributed to the breaking of metal-oxygen bond [36]. The 3MPS capped Fe(ZnO) indicated 3.88% and 40.75% weight loss at the temperature ranges of 20–150 °C and 410–470 °C, respectively. The first degradation path was attributed to the removal of adsorbed –OH groups and the second degradation was due to the removal of the organic content of 3MPS. Thermal profile of co-polymerized poly(styr-co-MMA)-3MPS-Fe(ZnO) showed a distinct weight loss of 79.65% in the temperature range of 367–450 °C ascribed to the removal of polymeric content. No further weight loss indicated that organic polymer chain completely degraded at this temperature and the curve became linear as the temperature increased [36]. The EDA functionalized poly(styr-co-MMA)-3MPS-Fe(ZnO) showed a gradual weight loss of 24.61% up to 380 °C owing to the breakage of surface grafting groups along with –OH group from moisture. Another distinct weight loss of 60.05% was observed when heated up to 450 °C presumably due to the removal of polymeric organic groups. Two layer degradation path with weight losses of 30.32% at 100 °C and 30.54% at 250 °C were due to decomposition of surface adhering groups (–NH_2 and –SO_3H), polymeric backbone and residual organic mass [37]. It is clearly evident from the thermogravimetric curve that sulphonation has improved the stability of the microsphere and it became stable only after 300 °C with no further weight loss.

3.6. VSM

The magnetic properties of the prepared samples were examined by B-H curves of the samples taken at room temperature (Figure 3). The Fe(ZnO) and 3-MPS-Fe(ZnO) displayed good hysteresis curves with magnetic saturation (M_s) values of 3.89 emu/g and

1.5 emu/g, respectively. The magnetic curves indicated the induction of magnetization in the diamagnetic ZnO ($\mu B = 0$) due to the successful incorporation of Fe in the ZnO lattice [38]. However, the M_s for Fe(ZnO) is low as compared to Fe ($M_s = 68.3$ emu/g) due to high proportion of ZnO than Fe (4% doping) in the Fe(ZnO). The decrease in M_s value of 3MPS-Fe(ZnO) than Fe(ZnO) is due to the capping of the magnetic zinc oxide surface with silane groups and it is supported by the earlier reports [38,39]. After polymerization reaction with styrene and methyl methacrylate, the saturation magnetization of 3MPS-Fe(ZnO) was further reduced to 0.2 emu/g. This behavior indicated a decrease in crystalline structure which affects the magnetic properties of the compounds. The shape of the hysteresis loop suggested ferromagnetic nature of the synthesized material [40]. EDA substituted poly (styr-co-MMA)-3MPS-Fe(ZnO) also exhibited magnetic character with distorted hysteresis loop. The abnormality in hysteresis curve is ascribed to the nature of surface adhering group which may alter the structure and morphology of the said material thereby influencing magnetic features. For sulphonated–EDA modified poly(styr-co-MMA)-3MPS-Fe(ZnO), a straight hysteresis curve is due to the poor crystallinity and diamagnetic contributions of the functionalized polymeric groups in consistent with the [41]. However, the curve still displayed a positive saturation magnetization indicating it a weakly magnetic material [39]. The magnetic characteristics of the synthesized samples suggest the easy separation of the adsorbent after the sorption of desired pollutant.

3.7. Adsorption Studies

The synthesized MFZPI and SMFZPI were employed as sorbents to monitor maximum sorption for Cr(III) and fluorescein from water solutions in single batch sorption system. The following parameters were regulated in order to investigate the strength of ion exchange adsorption.

3.7.1. Effect of pH

The ability of synthesized EDA modified MFZPI and sulphonated MFZPI to adsorb Cr(III) and fluorescein from aqueous media was investigated by regulating pH of the solution and keeping other factors (contact time, initial concentration, temperature, adsorbent dose) constant. The results indicated that pH regulation of Cr(III) and fluorescein solution greatly affected the adsorption capacity of the functionalized polymer microspheres (Figure 4). The maximum removal of metal/dye with pH regulation is characterized by point of zero charge (pH_{cpz}). It is the pH at which the sorbent behaves as a neutral specie, below this pH the sorbent acquires positive charge due to deprotonation and above this increased amount of $–OH^-$ ions encourage the sorbent to behave as negatively charged material [42]. The pH_{cpz} was found to be 10 for aminated MFZPI and 4 for sulphonated SMFZPI sorbent. The MFZPI contained surface positive charges which depicted maximum fluorescein sorption (1.84 mg/g) at pH = 6 due to large concentration of positive charges as the pH is lower than pH_{cpz}. Likewise, SMFZPI showed maximum adsorption of 2.6 mg/g at pH = 2. The maximum adsorption of fluorescence at acidic pH is based on the fact that it electrostatically interacts with the positively charged sorbent surface due to its anionic nature [43]. This electrostatic interaction decreases as the pH is increased because increase in pH decreases the positive charge thereby electrostatic repulsions start dominating. For Cr(III), the maximum adsorption (q_e) of 1.77 mg/g and 2.63 mg/g were observed at pH = 12 and pH = 8 for MFZPI and SMFZPI, respectively. According to pH_{cpz}, the SMFZPI ($pH_{cpz} = 4$) has shown maximum sorption for Cr(III) due to the increase in negative surface charges at $pH > pH_{cpz}$. However, the greater sorption of MFZPI than SMFZPI is attributed to the fact that spontaneous adsorption of the cationic metal ion occurs owing to the increasingly positive charge surface ($pH < pH_{cpz}$) and strong hydrogen bonding starts operating in addition to the electrostatic interactions [44]. The results were found to be in accordance with the reported sorbents for the removal Cr(III) ions and fluorescein dye [45,46].

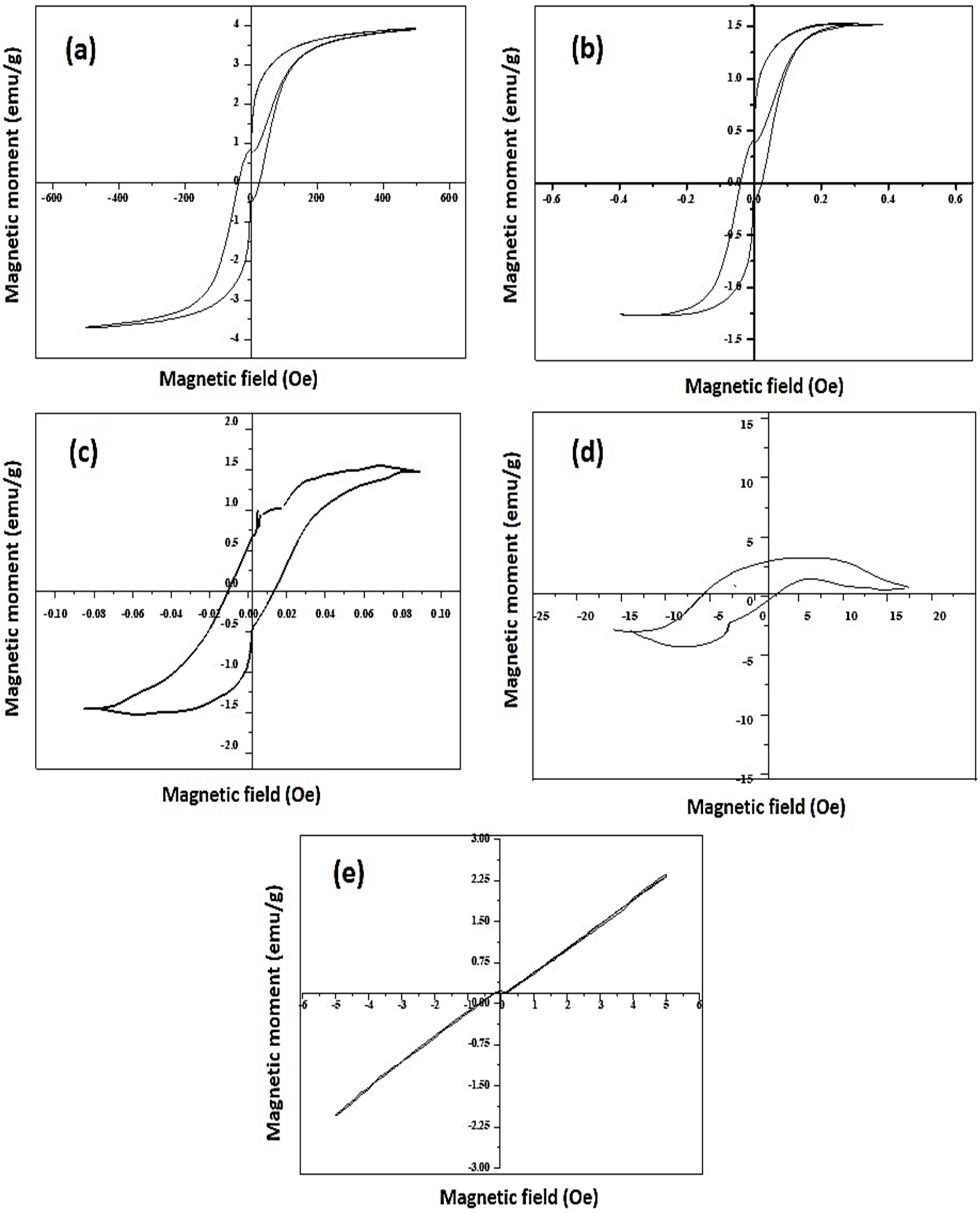

Figure 3. B-H hysteresis loops of (**a**) Fe(ZnO), (**b**) 3-MPS-Fe(ZnO), (**c**) poly(styr-co-MMA)-3MPS-Fe(ZnO), (**d**) EDA-poly(styr-co-MMA)-3MPS-Fe(ZnO) (MFZPI), and (**e**) Sulphonated-EDA-poly(styr-co-MMA)-3MPS-Fe(ZnO) (SMFZPI).

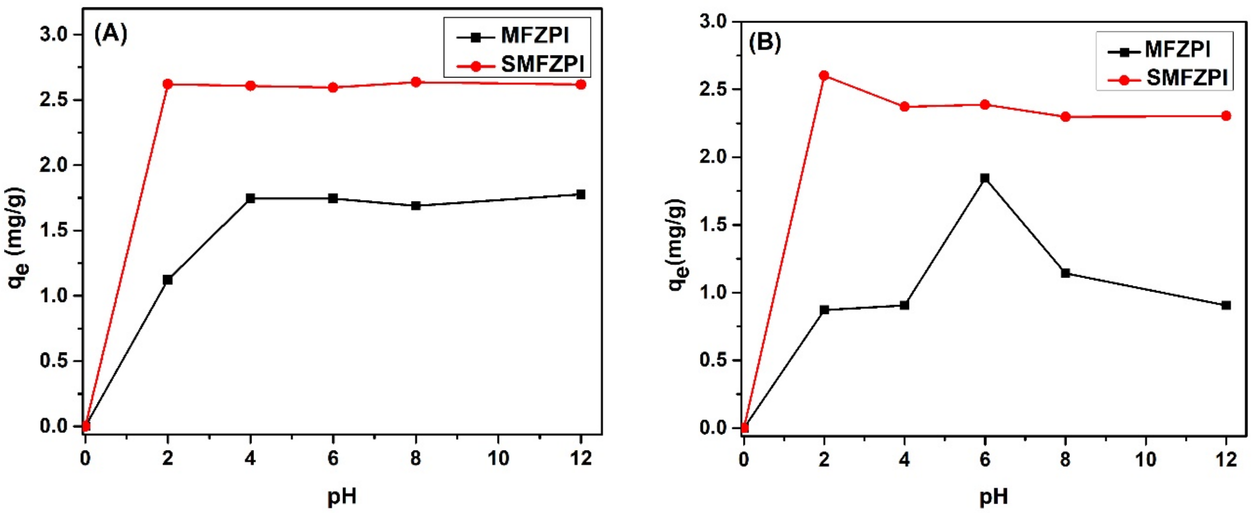

Figure 4. The influence of pH (2–12) on the sorption capacity of MFZPI and SMFZPI against (**A**) Cr(III), and (**B**) Fluorescein (solution concentration = 10 mg/L, sorbent dose = 30 mg, and temperature = 293K).

3.7.2. Effect of Contact Time

The influence of contact time of the sorbent on the adsorption of Cr(III) and fluorescein was investigated at different contact times i.e., 20, 40, 60, 80, 100, 120, 140 and 180 min using 10 ppm of initial metal/dye concentration and 30 mg of each ion exchange sorbent. For Cr(III), the pH was adjusted at 12 for MFZPI and at 8 for SMFZPI whereas in case of fluorescein pH = 6 and pH = 2 were maintained for MFZPI and SMFZPI, respectively. The adsorption curves of MFZPI and SMFZPI against Cr(III) as a function of time are shown in Figure 5. The maximum adsorption (q_e) of 0.69 mg/g was observed within first 40 min of MFZPI contact whereas SMFZPI has shown maximum adsorption (q_e) of 2.67 mg/g in first 20 min. This difference of contact time on the adsorption efficiency of Cr(III) is attributed to the surface charges of MFZPI and SMFZPI. The MFZP1 has taken greater time with smaller adsorption capacity due to the similar positive charge distribution on MFZPI and Cr(III). Whereas, the negative charges on SMFZPI due to $–SO_3H$ groups quickly adsorbed the positively charged Cr(III) in only 20 min due to opposite charges attraction. Bekchanov et al. reported similar adsorption behavior for the Cr(III) ions using nitrogen- and sulfur-containing polyampholyte ion exchangers with maximum adsorption capacity of 3.97 mmol/g [47]. For anionic dye, fluorescein, the MFZPI has shown maximum adsorption of 1.63 mg/g in first 20 min whereas SMFZPI revealed maximum adsorption of 1.428 mg/g after 60 min of contact between the dye and sorbent. The MFZPI showed high adsorption in just 20 min for anionic dye due to the opposite charges on the sorbent and substrate thus working as anion exchange polymer. Contrarily, the negatively charged SMFZPI and anionic fluorescence having similar charge showed least interaction between sorbent and sorbate. The literature on the adsorptive removal of fluorescein using ion exchange adsorbents support our findings [48,49]. It has also been observed that when contact times were further increased for Cr(III) and fluorescence, the adsorption capacities decreased and finally became constant. The high sorption capacities at less contact time are due to the large number of vacant sites available on the surface of the adsorbent. The graph becomes linear as the time increases due to the non-availability of vacant spaces and the repulsive forces operates for the upcoming ions by the already entrapped Cr(III)/fluorescein ions [18].

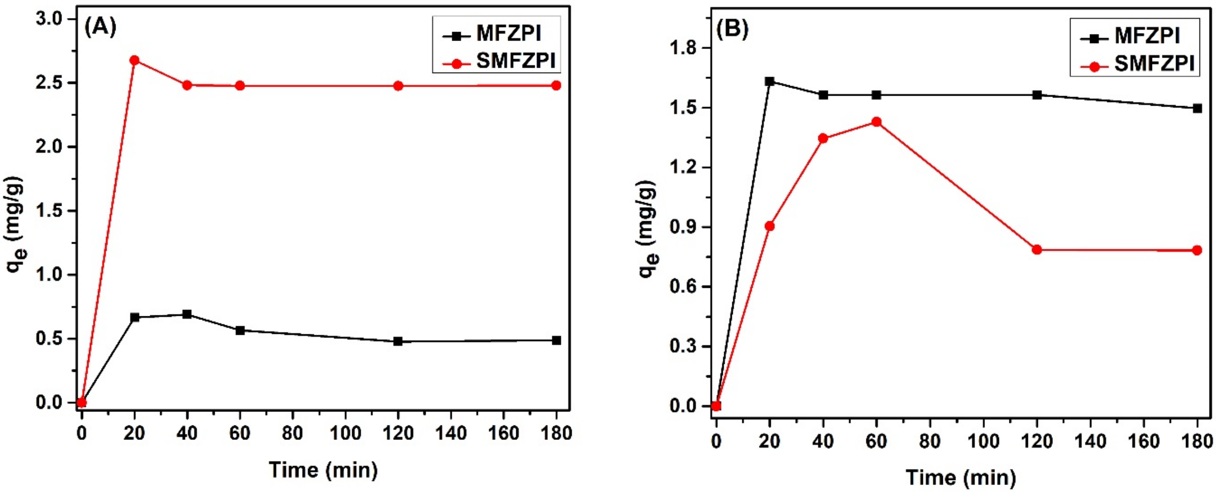

Figure 5. The influence of contact time (20–180 min) on the sorption capacity of MFZPI and SMFZPI against (**A**) Cr(III), and (**B**) Fluorescein (solution concentration = 10 mg/L, sorbent dose = 30 mg, and temperature = 293K).

3.7.3. Effect of Initial Metal/Dye Concentration

The effect of initial concentration of Cr(III) and fluorescein on the adsorption capacities of MFZPI and SMFZPI was studied at various initial concentrations (20–80 ppm) of metal/dye by keeping the sorbent dose (30 mg) constant (Figure 6). The MFZPI has shown maximum adsorption of 0.33 mg/g for the Cr(III) at 60 ppm whereas for SMFZPI, q_e= 16.79 mg/g was observed at 80 ppm. It is clearly evident from these values that adsorption of the Cr(III) has increased by increasing the initial concentration of the Cr(III). For fluorescein, similar trend was observed with highest adsorptions of 9.22 mg/g and 12.03 mg/g for MFZPI and SMFZPI, respectively, at 80 ppm. Initially the presence of multiple binding sites facilitated the maximum adsorption of the metal/dye but further increase in concentration led to the less sorption due to competition established for binding sites between adsorbent and adsorbate, afterwards graph becomes linear gradually [50]. However, SMFZPI has shown better ion exchange sorption for metal/dye than MFZPI due to the presence of both amine and sulphonic groups.

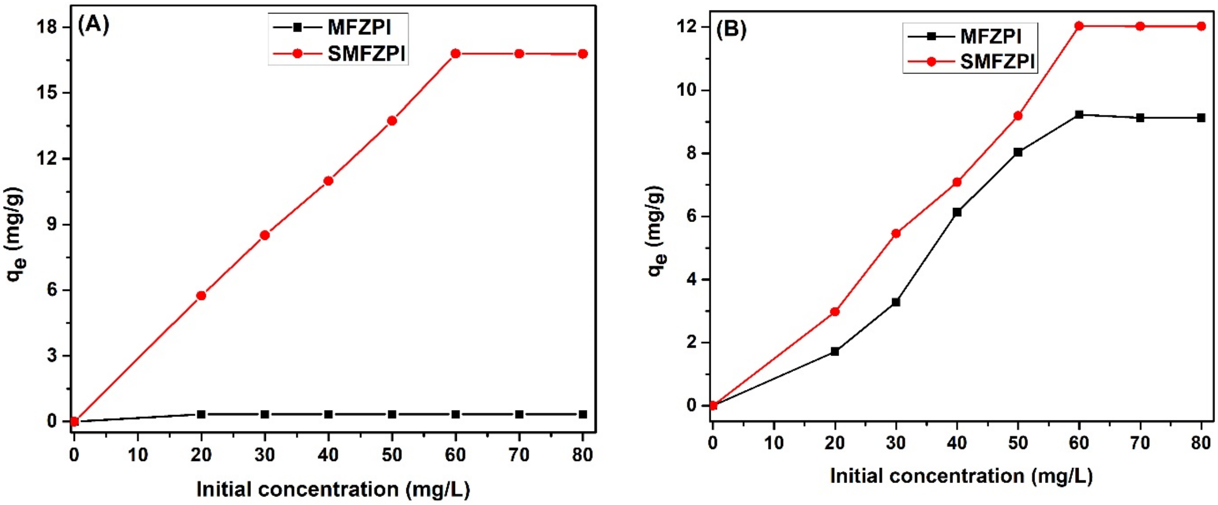

Figure 6. The influence of initial concentration (10–80 ppm) of metal/dye on the sorption capacity of MFZPI and SMFZPI against (**A**) Cr(III), and (**B**) Fluorescein (sorbent dose = 30 mg, and temperature = 293K).

3.7.4. Effect of Temperature

The rate of adsorption is considerably affected by the changes in temperature. The interaction between sorbent-sorbate interfaces were studied in the temperature range of 293–333K (Figure S5). The removal of Cr(III) by MFZPI depicted a rise in q_e by increasing temperature (Figure S5A). The sorption of Cr(III) and fluorescein by SMFZPI and of fluorescein by MFZPI followed an inverse relation with temperature i.e., the sorption capacity decreased when temperature was increased. The maximum adsorption (2.39 mg/g) of Cr(III) was observed by SMFZPI at 293K whereas MFZPI has only shown q_e = 1.81 mg/g at the similar temperature. For fluorescein, SMFZPI indicated maximum adsorption of 2.52 mg/g at 293K which is significantly greater than the fluorescein adsorption by MFZPI 0.96 mg/g at the same temperature. The decrease in adsorption capacity with increase in temperature is attributed to the fast movement of molecules at higher temperature which can reverse the sorption process [45].

3.8. Mathematical Modelling

The mathematical modelling of the optimized adsorption data is very important to compare the relative sorptive efficiencies of the synthesized materials for commercial scale applications.

3.8.1. Kinetic Studies

The kinetic modelling helps to understand the underlying reaction mechanism suitable for the adsorption process. The adsorption kinetics was evaluated by considering the contact time data of sorbent–sorbate species. Pseudo first-order, pseudo second-order, Elovich and intraparticle diffusion models were applied to study the rate of adsorption for Cr(III) and fluorescein by synthesized MFZPI and SMFZPI. The obtained parameters of these kinetic models and regression coefficient (R^2) values are given in Table 1. The Elovich model is based on the fact that increase in sorption sites favours the exponential increase in adsorption owing to the multiple interactions between sorbent and sorbate [51]. The plot of lnt vs. q_t provided the values of Elovich constants and the obtained values of a and b (Equation (3)) represented satisfactory adsorption of the metal/dye on the adsorbent surface. However, the correlation coefficient R^2 values were quite small which reflected that absorption data is not supported by Elovich model. The pseudo first-order kinetics was applied by plotting ln ($q_e - q_t$) vs. t according to Equation (4) and it showed large difference (D%) between calculated and experimental values with $R^2 < 0.7$ indicating that rate of Cr(III) and fluorescein adsorption was not governed by pseudo first-order kinetics. The plot between t/q_t vs. t as per Equation (5) provided the pseudo-second order kinetic model. The graph depicted small difference (D%) between experimental and calculated sorption capacities (q_e, mg/g) with good regression (R^2) values in the range of 0.997–0.999 indicating the rate of Cr(III) and fluorescein sorption by MFZPI and SMFZPI followed pseudo second-order kinetics. According to pseudo second-order model, rate of adsorption depends upon the adsorption capacity instead of adsorbate concentration. It is also established from the literature that adsorption of metal/dye usually follows pseudo second-order kinetics [52,53]. However, the aforementioned models cannot identify the diffusion mechanisms; therefore, intraparticle diffusion model was applied using Equation (6). It could be inferred that MFZPI and SMFZPI followed boundary layer diffusion rather than intraparticle diffusion as a rate determining step because the intraparticle diffusion model showed $R^2 < 0.82$ and $K_{in} < 1$. Recently, Dinh et al., also reported that adsorption of a cationic dye and Cr(III) followed boundary layer diffusion along with intraparticle diffusion [54].

Table 1. Kinetic constants for the adsorption of Cr(III) and fluorescein on the surfaces of MFZPI and SMFZPI.

Kinetic Models	**Type of Adsorbent**			
	MFZPI		**SMFZPI**	
	Cr(III)	**Fluorescein**	**Cr(III)**	**Fluorescein**
Elovich kinetics				
α (g mg^{-1} min^{-1})	1.54×10^4	2.11×10^{14}	0.362	0.008
β (g mg^{-1})	−15.01	20.36	−0.135	−0.939
R^2	0.522	0.793	0.56	0.108
Pseudo first-order kinetics				
K_1 (min^{-1})	−0.0129	0.0062	0.006	−0.001
q_e(mg g^{-1})	0.03	0.224	0.453	0.521
R^2	0.6588	0.12	0.294	0.016
Pseudo second-order kinetics				
K_2 (g mg^{-1} min^{-1})	−0.244	−0.26	−0.534	−0.102
q_e(mg g^{-1})	0.45	1.49	2.469	0.728
R^2	0.9972	0.999	0.999	0.978
Intraparticle diffusion kinetics				
K_{in} (mg g^{-1} $min^{-1/2}$)	−0.0246	−0.011	−26.2	−5.795
R^2	0.8116	0.7739	0.418	0.188

3.8.2. Equilibrium Isothermal Studies

Isothermal modeling is employed to study the interaction between the adsorbent and adsorbate in their equilibrium state. Langmuir, Freundlich and Dubrinin-Radulskawich isothermal models were applied on the concentration data obtained experimentally with the parameters are given in Table 2. Langmuir isothermal plot of C_e/q_e versus q_e depicted that only Cr(III) uptake by MFZPI followed monolayer isotherm with regression coefficient value equal to 1 with maximal adsorption capacity (q_m) of 0.33 mg/g. This low q_{max} is attributed to the repulsive forces between positive cation (Cr(III)) and amine modified MFZPI. However, q_m of Cr(III) by SMFZPI was high i.e., 52.35 mg/g due to attractive forces between the adsorbate and adsorbent surface but showed no applicability of Langmuir isotherm (R^2 = 0.65). The maximum sorption of fluorescein was 3.419 mg/g by MFZPI and 10.49 mg/g by SMFZPI despite that they did not follow monolayer isotherm due to low R^2 values ($R^2 < 0.7$). Freundlich isotherm establishes the idea of multilayer adsorption obtained by plotting ln q_e versus ln C_e and explains the heterogeneous adsorption of Cr(III) and fluorescein with coefficient of determination R^2 = 0.97. The Freundlich parameter "n" represents the efficiency of adsorption process and its value from 0–2 signifies good sorption [55]. The n values of both sorbents lie in this range for Cr(III) and fluorescein as evident from the Table 2, predicting that synthesized polymerized microspheres are good sorbents for the under studied pollutants. The SMFZPI has shown higher values of Freundlich parameter (K_F) than MFZPI indicating the effective bonding of SMFZPI with the pollutants. Dubinin–Radushkevich isotherm is distinctive than Langmuir and Freundlich isotherms in terms of its contribution in estimating the adsorption energy of the system. This isotherm is based on the assumption of multilayer adsorption followed by Vander Waal's interactions [18]. The mean adsorption energy (E) of the overall batch sorption predicts whether adsorption is physio-sorption or chemi-sorption. If value of E is less than 8 kJ mol^{-1} then physio-sorption takes place and if it is greater than 16 kJ mol^{-1} it indicates chemisorption [56]. Table 2 shows that all values of E are larger than 16 kJ mol^{-1} showing that process of chemisorption. The increasing order of chemisorption is as follows, MFZPI (Fluorescein) < SMFZPI (Fluorescein) < SMFZPI (Cr(III)) < MFZPI (Cr(III)).

Table 2. Isothermal parameters of Cr(III) and fluorescein adsorption by MFZPI and SMFZPI.

Isothermal Models	**Type of Adsorbent**			
	MFZPI		**SMFZPI**	
	Cr(III)	**Fluorescein**	**Cr(III)**	**Fluorescein**
Langmuir Isotherm				
K_L (L mg^{-1})	1×10^3	0.024	0.042	-0.021
q_m(mg g^{-1})	0.33	3.419	52.35	10.49
R^2	1	0.655	0.601	0.67
Freundlich Isotherm				
n	1.61×10^2	0.48	1.26	0.631
K_F (mg g^{-1})	0.335	-7.907×10^{-3}	2.541	0.073
R^2	0.851	0.989	0.974	0.948
D-R Isotherm				
ß ((mol^2·kJ^2)$^{-1}$)	-3×10^{-10}	8×10^{-5}	2×10^{-6}	3×10^{-5}
E (kJ mol^{-1})	4.09×10^4	79.36	500	129.19
q_m(mg g^{-1})	0.334	14.12	15.28	14.65
R^2	0.866	0.965	0.879	0.948

3.8.3. Thermodynamics

Thermodynamics of sorption process helps to determine the feasibility of the adsorption and heat changes of the system. The changes in thermodynamic parameters such as Gibbs free energy (ΔG°), entropy (ΔS°), and enthalpy (ΔH°) were calculated for the adsorption of Cr(III) and fluorescein by functionalized polymeric microspheres as adsorbents. The calculated values of ΔG° were found to be negative for the adsorption of Cr(III) and fluorescein by MFZPI which indicated that sorption process was spontaneous. However, large positive ΔG° values for the adsorption of Cr(III) and fluorescein by SMFZPI showed that adsorption process was non-spontaneous. The favorability of ion exchange process was estimated by plot of Gibb's free energy against T (K) with good correlation coefficient value i.e., $R^2 > 0.9$. The Cr(III) sorption by MFZPI indicated an exothermic process (ΔH° = −412.93 kJ/mol) with decreased entropy (ΔS° = −0.146 kJ/mol/K). Contrarily, the sorption of Cr(III) by SMFZPI and of fluorescein by MFZPI and SMFZPI indicated endothermic reactions with decreased randomness at sorbate—sorbent interfaces. Thermodynamic parameters are tabulated in Table 3. It can be conferred from the results that adsorption of Cr(III) and fluorescein by synthesized sorbents is chemisorption process which is effective for the removal of pollutants from waste water.

Table 3. Thermodynamic parameters of Cr(III) and fluorescein adsorption by MFZPI and SMFZPI.

Ion Exchange Adsorbent	**Temperature (K)**	**ΔG° (kJ/mol)**		**ΔS° (kJ/mol/K)**		**ΔH° (kJ/mol)**	
		Cr(III)	**Fluorescein**	**Cr(III)**	**Fluorescein**	**Cr(III)**	**Fluorescein**
MFZPI	293	−369.42	−6912	−0.146	24	−412.93	240
	313	−367.23	−7272				
	333	−364.31	−7752				
SMFZPI	293	334.27	235.86	0.084	0.079	359.40	259.56
	313	333.01	234.67				
	333	331.32	233.08				

The MFZPI adsorbent revealed higher adsorption towards fluorescein (q_e = 9.22 mg/g) than for Cr(III) (q_e = 0.33 mg/g). The expected low uptake of Cr(III) by MFZPI is due to repulsive forces between positively charged cation (Cr(III)) and amine modified MFZPI and vice versa. Therefore, due to quite low q_e, it is suggested that MFZPI is not suitable for Cr(III) sorption from water systems. On the other hand, SMFZPI depicted sorption capacities of 16.79 mg/g and 12.03 mg/g for Cr(III) and fluorescein, respectively. This change in the sorption behavior of SMFZPI is due to the presence of both amine and sulphonate groups on polymer network. The presence of negatively and positively charged functional groups allows the sorbent to capture both cationic and anionic pollutants, therefore, increasing the overall ion exchange performance of the SMFZPI. These findings were in agreement with the reported literature on the functionalized sorbents for the removal of metals and organic dyes (Table 4). For instance, Ceglowski et al. reported a polymeric adsorbent, 1,3,5-tris(6-isocyanatohexyl)-1,3,5-triazinane-2,4,6-trione-PEHA (PEHA = pentaethylenehexamine) for the removal of Cr(III) with an equilibrium adsorption capacity of 3.15 mg/g [57]. Another study reported amino silica microspheres for the adsorption of fluorescein with an equilibrium adsorption capacity of 84.86 mg/g [48]. The different sorption capacities of reported adsorbents with our work are attributed to the different types and ratios of surface modifying groups. It can be suggested that modified polymer microspheres can be effectively tailored by different groups and therefore, could be employed as potential adsorbents for the removal of toxic metals/dye.

Table 4. Comparision of maximum adsorption capacities of some reported sorbents for the removal of toxic metals and fluorescein dye.

Adsorbent	Metal/dye	Quantity Adsorbed (mg/g)	References
Amino functionalized PAA-coated Fe_3O_4 nanoparticles	Cu^{2+}	12.43	[58]
AMP-Polyacrylonitrile	Co^{2+}	9.43	[59]
α-Fe_2O_3-impregnated chitosan beads	As^{3+}	6.18	[60]
Prussian Blue derivate- modified SBA-15 (SBA-15@FC)	Cs^{+}	13.90	[61]
PB-IE-PVA-ALG	Cs^{+}	3.33	[62]
HDI-IC-Diethylenetriamine	Cr^{3+} Co^{2+}	4.12 15.87	[57]
1,3,5-tris(6-isocyanatohexyl)-1,3,5-triazinane-2,4,6-trione-DETA	Cr^{3+}	9.80	[57]
Juniperusmicroparticles (JH) Solenostemmaargel (Del) Hayne (SH)	Fluorescein Fluorescein	2.91 2.565	[63]
MFZPI	Cr^{3+} Fluorescein	0.33 9.224	This study
SMFZPI	Cr^{3+} Fluorescein	16.79 12.03	This study

Note(s): PAA: Polyacrylic acid; AMP: Ammonium molybdophosphate; PB: Prussian blue; IE: Ion exchange; PVA: poly(vinyl alcohol) (PVA); ALG: Alginate; HDI-IC: 1,3,5-tris(6-isocyanatohexyl)-1,3,5-triazinane-2,4,6-trione; DETA: Diethylenetriamine.

4. Conclusions

In the present work, poly(styr-co-MMA) microspheres embedded with 3MPS-Fe(ZnO) have been synthesized by modified suspension polymerization. These polymeric hybrid microspheres were functionalized using low cost and easily available reagents i.e., ethylenediamine and sulphuric acid to induce cationic and anionic exchange properties. The results of various analytical techniques confirmed the successful functionalization with improved structural, optical, thermal, and morphological features. The adsorption of Cr(III) and fluorescein from aqueous solution using EDA and sulphonated modified polymer microspheres (MFZPI, SMFZPI) suggested their ion exchange properties for the adsorptive removal of pollutants. The mathematical modeling indicated pseudo second-order kinetics with multilayer adsorption supported by Freundlich isotherm. Moreover, a thermodynamically feasible ion exchange adsorption that followed heterogeneous adsorption with large mean free energy was observed. Therefore, a successful attempt has been made for designing a system that utilizes environment friendly, economical, and easily accessible approach to remove pollutants from the wastewater.

Supplementary Materials: The following supporting information can be downloaded at: https://www.mdpi.com/article/10.3390/w15091761/s1, Text S1: Materials and Methodology; Scheme S1: The schematic illustration of the series of steps involved in the synthesis of co-polymerized magnetic ZnO microspheres and their functionalization; Figure S1: FTIR spectra of (a) Fe(ZnO), (b) 3-MPS-Fe(ZnO), (c) poly(styr-co-MMA)-3MPS-Fe(ZnO), (d) EDA-poly(styr-co-MMA)-3MPS-Fe(ZnO) (MFZPI), and (e) Sulphonated-EDA-poly(styr-co-MMA)-3MPS-Fe(ZnO) (SMFZPI); Figure S2: UV-Vis spectra of (a) Fe(ZnO), (b) 3-MPS-Fe(ZnO), (c) poly(styr-co-MMA)-3MPS-Fe(ZnO), (d) EDA-poly(styr-co-MMA)-3MPS-Fe(ZnO) (MFZPI), and (e) Sulphonated-EDA-poly(styr-co-MMA)-3MPS-Fe(ZnO) (SMFZPI); Figure S3: EDX profiles of (a) Fe(ZnO), (b) 3-MPS-Fe(ZnO), (c) poly(styr-co-MMA)-3MPS-Fe(ZnO), (d) EDA-poly(styr-co-MMA)-3MPS-Fe(ZnO) (MFZPI), and (e) Sulphonated-EDA-poly(styr-co-MMA)-3MPS-Fe(ZnO) (SMFZPI); Figure S4: Thermogravimetric curves of (a) Fe(ZnO), (b) 3-MPS-Fe(ZnO), (c) poly(styr-co-MMA)-3MPS-Fe(ZnO), (d) EDA-poly(styr-co-MMA)-3MPS-Fe(ZnO) (MFZPI), and (e) Sulphonated-EDA-poly(styr-co-MMA)-3MPS-Fe(ZnO) (SMFZPI); Figure S5: The influence of temperature (293–333K) on the sorption capacity of MFZPI and SMFZPI against (A) Cr(III), and (B) Fluorescein (initial concentration = 10 mg/L, and sorbent dose = 30 mg).

Author Contributions: Conceptualization, S.F., M.I. and G.B.; methodology, S.F. and M.I.; software, S.F. and A.J.; validation, S.F. and M.I.; formal analysis, S.F., M.I. and S.L.; investigation, S.F.; resources, M.I.; data curation, S.F., M.I., F.K. and A.J.; writing—original draft preparation, S.F. and M.I.; writing—review and editing, F.K., A.J., S.L. and G.B.; visualization, M.I.; supervision, M.I.; project administration, M.I. All authors have read and agreed to the published version of the manuscript.

Funding: This research received no external funding.

Data Availability Statement: The data that support the findings of this study are available from the corresponding author, upon a request.

Acknowledgments: The authors would like to acknowledge the Home University of Pakistan for financial assistance in the research work.

Conflicts of Interest: The authors declare no conflict of interest.

References

1. Janjhi, F.A.; Ihsanullah, I.; Bilal, M.; Castro-Muñoz, R.; Boczkaj, G.; Gallucci, F. MXene-based materials for removal of antibiotics and heavy metals from wastewater—A review. *Water Resour. Ind.* **2023**, *29*, 100202. [CrossRef]
2. Fu, Y.; Wang, L.; Peng, W.; Fan, Q.; Li, Q.; Dong, Y.; Liu, Y.; Boczkaj, G.; Wang, Z. Enabling simultaneous redox transformation of toxic chromium (VI) and arsenic (III) in aqueous media—A review. *J. Hazard. Mater.* **2021**, *417*, 126041. [CrossRef] [PubMed]
3. Mohammad, A.; Singh, A.; Pal, D.B.; Alhazmi, A.; Haque, S.; Yoon, T.; Srivastava, N.; Gupta, V.K. Biological remediation technologies for dyes and heavy metals in wastewater treatment: New insight. *Bioresour. Technol.* **2022**, *343*, 126154.
4. Honarmandrad, Z.; Sun, X.; Wang, Z.; Naushad, M.; Boczkaj, G. Activated persulfate and peroxymonosulfate based advanced oxidation processes (AOPs) for antibiotics degradation—A review. *Water Resour. Ind.* **2022**, *29*, 100194. [CrossRef]
5. Askarniya, Z.; Rayaroth, M.P.; Sun, X.; Wang, Z.; Boczkaj, G. Degradation of bisphenol S—A contaminant of emerging concern-by synergistic ozone and percarbonate based AOP. *Water Resour. Ind.* **2023**, *29*, 100208. [CrossRef]
6. Fedorov, K.; Rayaroth, M.P.; Shah, N.S.; Boczkaj, G. Activated sodium percarbonate-ozone (SPC/O3) hybrid hydrodynamic cavitation system for advanced oxidation processes (AOPs) of 1,4-dioxane in water. *Chem. Eng. J.* **2023**, *456*, 141027. [CrossRef]
7. Ma, Y.; You, D.; Fang, Y.; Luo, J.; Pan, Q.; Liu, Y.; Wang, F.; Yang, W. Confined growth of MOF in chitosan matrix for removal of trace Pb(II) from reclaimed water. *Sep. Purif. Technol.* **2022**, *294*, 121223. [CrossRef]
8. Fang, Y.; Ren, G.; Ma, Y.; Wang, C.; Li, M.; Pang, X.; Pan, Q.; Li, J. Adsorption and reutilization of Pb (II) based on acid-resistant metal-organic gel. *Sep. Purif. Technol.* **2022**, *295*, 121253. [CrossRef]
9. Toyofuji, A.; Hano, N.; Yamaguchi, Y.; Wakiya, T.; Ihara, H.; Takafuji, M. Preparation of Hybrid Microspheres with Homogeneously Dispersed Nanosilica using In-situ Sol-Gel Reaction inside Polystyrene Matrix. *Chem. Lett.* **2022**, *51*, 639–642. [CrossRef]
10. Czyżowska, A.; Barbasz, A. A review: Zinc oxide nanoparticles–friends or enemies? *Int. J. Environ. Health Res.* **2022**, *32*, 885–901. [CrossRef]

11. Roy, S.; Ghosh, M.P.; Mukherjee, S. Introducing magnetic properties in Fe-doped ZnO nanoparticles. *Appl. Phys. A* **2021**, *127*, 1–9. [CrossRef]
12. Ali, M.A.; Mubarak, M.F.; Keshawy, M.; Zayed, M.A.; Ataalla, M. Adsorption of Tartrazine anionic dye by novel fixed bed Core-Shell-polystyrene Divinylbenzene/Magnetite nanocomposite. *Alex. Eng. J.* **2022**, *61*, 1335–1352. [CrossRef]
13. Zhao, Y.; Chen, T.; Sang, Y.N.; Tang, M.; Hu, G.W.; Han, X.B.; Gao, J.; Ma, R. Facile synthesis of magnetic CS-g-SPSS microspheres via electron beam radiation for efficient removal of methylene blue. *J. Saudi Chem. Soc.* **2021**, *25*, 101299.
14. Ashraf, R.; Riaz, S.; Kayani, Z.N.; Naseem, S. Structural and magnetic properties of iron doped ZnO nanoparticles. *Mater. Today Proc.* **2015**, *2*, 5384–5389. [CrossRef]
15. Bach, L.G.; Islam, M.R.; Kim, J.T.; Seo, S.; Lim, K.T. Encapsulation of Fe_3O_4 magnetic nanoparticles with poly (methyl methacrylate) via surface functionalized thiol-lactam initiated radical polymerization. *Appl. Surf. Sci.* **2012**, *258*, 2959–2966. [CrossRef]
16. Tai, Y.; Wang, L.; Gao, J.; Amer, W.A.; Ding, W.; Yu, H. Synthesis of Fe_3O_4@ poly (methylmethacrylate-co-divinylbenzene) magnetic porous microspheres and their application in the separation of phenol from aqueous solutions. *J. Colloid Interface Sci.* **2011**, *360*, 731–738. [CrossRef] [PubMed]
17. Chung, T.H.; Chang, J.Y.; Lee, W.C. Application of magnetic poly (styrene–glycidyl methacrylate) microspheres for immunomagnetic separation of bone marrow cells. *J. Magn. Magn. Mater.* **2009**, *321*, 1635–1638. [CrossRef]
18. Kanwal, A.; Rehman, R.; Imran, M. Adsorptive Detoxification of Congo Red and Brilliant Green Dyes Using Chemically Processed Brassica Oleracea Biowaste from Waste Water. *Adsorpt. Sci. Technol.* **2022**, *2022*, 9995335. [CrossRef]
19. Athar, M.; Farooq, U.; Aslam, M.; Salman, M. Adsorption of Pb (II) ions onto biomass from Trifolium resupinatum: Equilibrium and kinetic studies. *Appl. Water Sci.* **2013**, *3*, 665–672. [CrossRef]
20. Hassan, M.M.; Khan, W.; Azam, A.; Naqvi, A.H. Effect of size reduction on structural and optical properties of ZnO matrix due to successive doping of Fe ions. *J. Lumin.* **2014**, *145*, 160–166. [CrossRef]
21. Raja, K.; Ramesh, P.; Geetha, D. Structural, FTIR and photoluminescence studies of Fe doped ZnO nanopowder by co-precipitation method. *Spectrochim. Acta Part A Mol. Biomol. Spectrosc.* **2014**, *131*, 183–188. [CrossRef]
22. Pavia, D.L.; Lampman, G.M.; Kriz, G.S.; Vyvyan, J.A. Introduction to Spectroscopy. 2014. Available online: http://dl.iranchembook.ir/ebook/organic-chemistry-2753.pdf (accessed on 23 September 2022).
23. Feng, L.; Guan, G.; Li, C.; Zhang, D.; Xiao, Y.; Zheng, L.; Zhu, W. In situ synthesis of poly (methyl methacrylate)/graphene oxide nanocomposites using thermal-initiated and graphene oxide-initiated polymerization. *J. Macromol. Sci. Part A* **2013**, *50*, 720–727. [CrossRef]
24. Frizzo, M.S.; Feuser, P.E.; Berres, P.H.; Ricci-Júnior, E.; Campos, C.E.; Costa, C.; de Araújo, P.H.H.; Sayer, C. Simultaneous encapsulation of zinc oxide and octocrylene in poly (methyl methacrylate-co-styrene) nanoparticles obtained by miniemulsion polymerization for use in sunscreen formulations. *Colloids Surf. A Physicochem. Eng. Asp.* **2019**, *561*, 39–46. [CrossRef]
25. Denizli, A.; Özkan, G.; Arica, M.Y. Preparation and characterization of magnetic polymethylmethacrylate microbeads carrying ethylene diamine for removal of Cu (II), Cd (II), Pb (II), and Hg (II) from aqueous solutions. *J. Appl. Polym. Sci.* **2000**, *78*, 81–89. [CrossRef]
26. Ruziwa, D.; Chaukura, N.; Gwenzi, W.; Pumure, I. Removal of Zn^{2+} and Pb^{2+} ions from aqueous solution using sulphonated waste polystyrene. *J. Environ. Chem. Eng.* **2015**, *3*, 2528–2537. [CrossRef]
27. Kugarajah, V.; Sugumar, M.; Swaminathan, E.; Balasubramani, N.; Dharmalingam, S. Investigation on sulphonated zinc oxide nanorod incorporated sulphonated poly (1,4-phenylene ether ether sulfone) nanocomposite membranes for improved performance of microbial fuel cell. *Int. J. Hydrogen Energy* **2021**, *46*, 22134–22148. [CrossRef]
28. Aydın, C.; Abd El-sadek, M.; Zheng, K.; Yahia, I.; Yakuphanoglu, F. Synthesis, diffused reflectance and electrical properties of nanocrystalline Fe-doped ZnO via sol–gel calcination technique. *Opt. Laser Technol.* **2013**, *48*, 447–452. [CrossRef]
29. Chen, L.; Feng, T.; Wang, P.; Xiang, Y. Transition metal (Fe, Co) and organic silanol modified mesoporous titanium phosphates as catalysts for the oxidation of benzyl alcohol in water. *React. Kinet. Mech. Catal.* **2013**, *110*, 485–496. [CrossRef]
30. Abdullah, O.G.; Aziz, S.B.; Omer, K.M.; Salih, Y.M. Reducing the optical band gap of polyvinyl alcohol (PVA) based nanocomposite. *J. Mater. Sci. Mater. Electron.* **2015**, *26*, 5303–5309. [CrossRef]
31. Mahmoudi Khatir, N.; Abdul-Malek, Z.; Zak, A.K.; Akbari, A.; Sabbagh, F. Sol–gel grown Fe-doped ZnO nanoparticles: Antibacterial and structural behaviors. *J. Sol-Gel. Sci. Technol.* **2016**, *78*, 91–98. [CrossRef]
32. Javaid, A.; Imran, M.; Kanwal, F.; Latif, S.; Erben, M.F.; Noureen, S. Structural, optical and morphological investigation of bismuth substituted cerium ferrite: An efficient photocatalyst and dielectric material for various applications. *Mater. Chem. Phys.* **2022**, *291*, 126704. [CrossRef]
33. Kamaludin, R.; Abdul Majid, L.; Othman, M.H.D.; Mansur, S.; Sheikh Abdul Kadir, S.H.; Wong, K.Y.; Khongnakorn, W.; Puteh, M.H. Polyvinylidene Difluoride (PVDF) hollow fiber membrane incorporated with antibacterial and anti-fouling by Zinc Oxide for water and wastewater treatment. *Membranes* **2022**, *12*, 110. [CrossRef] [PubMed]
34. Chen, Z.; Peng, K.; Mi, Y. Preparation and properties of magnetic polystyrene microspheres. *J. Appl. Polym. Sci.* **2007**, *103*, 3660–3666. [CrossRef]
35. Wei, X.; Cui, L.; Meng, Q.; Zheng, J.; Ye, Z. Adsorption of Cr (VI) on 1,2-ethylenediamine-aminated macroporous polystyrene particles. *Vaccum* **2013**, *89*, 1–6.
36. Patel, N.A.; Patel, I.B.; Bharat, V.L. Structural, thermal and chemical studies of Mn doped ZnO nanoparticles synthesized by Co-precipitation method. *Mater. Today Proc.* **2021**, *46*, 2277–2280. [CrossRef]

37. Maji, P.; Choudhary, R.B.; Majhi, M. Polymeric phase change nanocomposite (PMMA/Fe: ZnO) for electronic packaging application. *Appl. Phys. A* **2018**, *124*, 1–11. [CrossRef]
38. Valentin, C.B.S.; Silva, R.L.d.S.; Banerjee, P.; Franco, A. Investigation of Fe-doped room temperature dilute magnetic ZnO semiconductors. *Mater. Sci. Semicond. Process.* **2019**, *96*, 122–126. [CrossRef]
39. Castro-Lopes, S.; Guerra, Y.; Silva-Sousa, A.; Oliveira, D.; Gonçalves, L.; Franco, A.; Padrón-Hernández, E.; Peña-Garcia, R. Influence of pH on the structural and magnetic properties of Fe-doped ZnO nanoparticles synthesized by sol gel method. *Solid State Sci.* **2020**, *109*, 106438. [CrossRef]
40. Nisticò, R.; Cesano, F.; Garello, F. Magnetic materials and systems: Domain structure visualization and other characterization techniques for the application in the materials science and biomedicine. *Inorganics* **2020**, *8*, 6. [CrossRef]
41. Kulak, A.N.; Grimes, R.; Kim, Y.-Y.; Semsarilar, M.; Anduix-Canto, C.; Cespedes, O.; Armes, S.P.; Meldrum, F.C. Polymer-directed assembly of single crystal zinc oxide/magnetite nanocomposites under atmospheric and hydrothermal conditions. *Chem. Mater.* **2016**, *28*, 7528–7536. [CrossRef]
42. Binh, Q.A.; Nguyen, H.-H. Investigation the isotherm and kinetics of adsorption mechanism of herbicide 2,4-dichlorophenoxyacetic acid (2,4-D) on corn cob biochar. *Bioresour. Technol. Rep.* **2020**, *11*, 100520. [CrossRef]
43. Rehman, R.; Salariya, B.; Mitu, L. Batch scale adsorptive removal of brilliant green dye using Trapa natans peels in cost effective manner. *Rev. Chim.* **2016**, *67*, 1333–1337.
44. Salleh, M.A.M.; Mahmoud, D.K.; Karim, W.A.W.A.; Idris, A. Cationic and anionic dye adsorption by agricultural solid wastes: A comprehensive review. *Desalination* **2011**, *280*, 1–13. [CrossRef]
45. Bai, C.; Wang, L.; Zhu, Z. Adsorption of Cr(III) and Pb(II) by graphene oxide/alginate hydrogel membrane: Characterization, adsorption kinetics, isotherm and thermodynamics studies. *Int. J. Biol. Macromol.* **2020**, *147*, 898–910. [CrossRef]
46. Oladipo, A.A.; Ifebajo, A.O. Highly efficient magnetic chicken bone biochar for removal of tetracycline and fluorescent dye from wastewater: Two-stage adsorber analysis. *J. Environ. Manag.* **2018**, *209*, 9–16. [CrossRef] [PubMed]
47. Bekchanov, D.; Kawakita, H.; Mukhamediev, M.; Khushvaktov, S.; Juraev, M. Sorption of cobalt (II) and chromium (III) ions to nitrogen-and sulfur-containing polyampholyte on the basis of polyvinylchloride. *Polym. Adv. Technol.* **2021**, *32*, 2700–2709. [CrossRef]
48. Melnyk, I.V.; Tomina, V.V.; Stolyarchuk, N.V.; Seisenbaeva, G.A.; Kessler, V.G. Organic dyes (acid red, fluorescein, methylene blue) and copper (II) adsorption on amino silica spherical particles with tailored surface hydrophobicity and porosity. *J. Mol. Liq.* **2021**, *336*, 116301. [CrossRef]
49. Olorunyomi, J.F.; Liu, T.; Ho, C.-K.; Li, C.-Y.V.; Chan, K.-Y. Imparting UiO-66 with fast cation exchange property via sulfonating organic linkers for selective adsorption. *Sep. Purif. Technol.* **2021**, *260*, 118219. [CrossRef]
50. Cheruiyot, G.K.; Wanyonyi, W.C.; Kiplimo, J.J.; Maina, E.N. Adsorption of toxic crystal violet dye using coffee husks: Equilibrium, kinetics and thermodynamics study. *Sci. Afr.* **2019**, *5*, e00116. [CrossRef]
51. Ayawei, N.; Godwin, J.; Wankasi, D. Synthesis and sorption studies of the degradation of Congo Red by Ni-Fe layered double hydroxide. *Int. J. Appl. Chem. Sci. Res.* **2015**, *13*, 1197–1217.
52. Naghizadeh, A.; Ghafouri, M.; Jafari, A. Investigation of equilibrium, kinetics and thermodynamics of extracted chitin from shrimp shell in reactive blue 29 (RB-29) removal from aqueous solutions. *Desalination Water Treat.* **2017**, *70*, 355–363. [CrossRef]
53. Chakraborty, R.; Verma, R.; Asthana, A.; Vidya, S.S.; Singh, A.K. Adsorption of hazardous chromium (VI) ions from aqueous solutions using modified sawdust: Kinetics, isotherm and thermodynamic modelling. *Int. J. Environ. Anal. Chem.* **2021**, *101*, 911–928. [CrossRef]
54. Dinh, V.-P.; Le, H.M.; Nguyen, V.-D.; Dao, V.-A.; Hung, N.Q.; Tuyen, L.A.; Lee, S.; Yi, J.; Nguyen, T.D.; Tan, L. Insight into the adsorption mechanisms of methylene blue and chromium (III) from aqueous solution onto pomelo fruit peel. *RSC Adv.* **2019**, *9*, 25847–25860. [CrossRef] [PubMed]
55. Latif, S.; Rehman, R.; Imran, M.; Hira, U.; Iqbal, S.; Akram, M.; Mitu, L.; Alsantali, R.I.; Al-thagafi, Z.T. Use of Green Chemistry for Amputation of Chromium Ions from Wastewater by Alkali-Treated Composts of Fruit Peels in Economical Way. *J. Chem.* **2022**, *2022*, 9924164. [CrossRef]
56. Bhatt, R.R.; Shah, B.A. Sorption studies of heavy metal ions by salicylic acid–formaldehyde–catechol terpolymeric resin: Isotherm, kinetic and thermodynamics. *Arab. J. Chem.* **2015**, *8*, 414–426. [CrossRef]
57. Cegłowski, M.; Gierczyk, B.; Frankowski, M.; Popenda, Ł. A new low-cost polymeric adsorbents with polyamine chelating groups for efficient removal of heavy metal ions from water solutions. *React. Funct. Polym.* **2018**, *131*, 64–74. [CrossRef]
58. Huang, S.-H.; Chen, D.-H. Rapid removal of heavy metal cations and anions from aqueous solutions by an amino-functionalized magnetic nano-adsorbent. *J. Hazard. Mater.* **2009**, *163*, 174–179. [CrossRef] [PubMed]
59. Park, Y.; Lee, Y.-C.; Shin, W.S.; Choi, S.-J. Removal of cobalt, strontium and cesium from radioactive laundry wastewater by ammonium molybdophosphate–polyacrylonitrile (AMP–PAN). *Chem. Eng. J.* **2010**, *162*, 685–695. [CrossRef]
60. Liu, B.; Wang, D.; Li, H.; Xu, Y.; Zhang, L. As (III) removal from aqueous solution using α-Fe_2O_3 impregnated chitosan beads with As(III) as imprinted ions. *Desalination* **2011**, *272*, 286–292. [CrossRef]
61. Qian, J.; Ma, J.; He, W.; Hua, D. Facile synthesis of prussian blue derivate-modified mesoporous material via photoinitiated thiol–ene click reaction for cesium adsorption. *Chem. Asian J.* **2015**, *10*, 1738–1744. [CrossRef]

62. Lai, Y.-C.; Chang, Y.-R.; Chen, M.-L.; Lo, Y.-K.; Lai, J.-Y.; Lee, D.-J. Poly (vinyl alcohol) and alginate cross-linked matrix with immobilized Prussian blue and ion exchange resin for cesium removal from waters. *Bioresour. Technol.* **2016**, *214*, 192–198. [CrossRef] [PubMed]
63. Al-Senani, G.M.; Al-Kadhi, N.S. Studies on adsorption of fluorescein dye from aqueous solutions using wild herbs. *Int. J. Anal. Chem.* **2020**, *2020*, 8019274. [CrossRef] [PubMed]